

Jagiellonian University
Faculty of Physics, Astronomy and Applied Computer Science



FEASIBILITY STUDIES OF MEASUREMENTS OF
ANNIHILATION PHOTONS POLARIZATION WITH THE
J-PET DETECTOR

Master thesis

Author:

Nikodem Krawczyk
nikodem.krawczyk@gmail.com

Thesis supervisor:

prof. dr hab. Paweł Moskal

Cracow, September 8, 2016

Abstract

The purpose of this thesis was to check the feasibility of the Jagiellonian Positron Emission Tomograph (J-PET) to measure the polarisation of the gamma quanta originating from the decays of ortho-positronium atoms. The studies were conducted via analysis of the results of Monte Carlo simulation of annihilation of ortho-positronium into three gamma quanta which was carried out using GATE software. The source code of this program has been modified to implement ortho-positronium decaying into three gamma quanta with the appropriate distribution of four-momenta. In this thesis a way of measuring the polarization of individual gamma quanta with the analysis and the uncertainty of such a measurement was discussed. Analysis of quantities such as: (i) Compton scattering angle of annihilation gamma quanta, (ii) the angles between the plane of ortho-positronium decay and scattering plane of gamma quantum and (iii) the angle between the normal vector to the decay plane and the axis of symmetry of the detector was performed. Understanding the distribution of these quantities and making sure that we have experimental access to all possible configurations is an essential element of quantum measurements. The future measurement of quantities simulated in this thesis will allow the deeper understanding of the phenomenon of quantum entanglement and will allow to test discrete symmetries in the leptonic sector.

Abstrakt (PL)

Celem niniejszej pracy było sprawdzenie możliwości dokonania pomiaru polaryzacji kwantów gamma pochodzących z rozpadów atomów orto-pozytonium za pomocą Jagiellońskiego Tomografu Pozytonowego (J-PET). Badania przeprowadzono za pomocą analizy wyników symulacji Monte Carlo rozpadu orto-pozytonium na trzy kwanty gamma, wykonanej przy użyciu programu GATE. Kod źródłowy tego programu został zmodyfikowany w celu implementacji źródła trzech kwantów gamma z odpowiednim rozkładem czteropędów. W pracy przedyskutowany został sposób pomiaru polaryzacji pojedynczych kwantów gamma wraz z analizą niepewności takiego pomiaru. Przeprowadzona została analiza wielkości takich jak: (i) kąt rozproszenia Comptona anihilacyjnych kwantów gamma, (ii) kąty pomiędzy płaszczyzną rozpadu orto-pozytonium i płaszczyzną rozproszenia kwantu gamma oraz (iii) kąt między

płaszczyzną rozpadu a osią symetrii detektora. Poznanie rozkładów tych wielkości oraz upewnienie się, że posiadamy eksperymentalny dostęp do wszystkich możliwych konfiguracji jest niezbędnym elementem pomiarów kwantowych. Późniejsze pomiary wielkości wysymulowanych na potrzeby tej pracy pozwolą na głębsze zrozumienie fenomenu jakim jest splątanie kwantowe oraz umożliwią badanie symetrii dyskretnych w obszarze leptonowym.

Contents

1	Introduction	1
2	J-PET detector	3
2.1	Current solutions in positron emission tomography	3
2.2	New concept	5
3	Research methods	7
3.1	Positronium	7
3.2	Measurement of linear polarization of photons	7
4	Description of the simulation	11
5	Validation of simulation	13
6	Results	18
6.1	Conclusions	22
7	Summary	24
	Bibliography	25

Introduction

Existence of the Universe is possible due to excess of matter over antimatter. That asymmetry had to occur at the early stage of the evolution, during baryogenesis. Processes driven by strong, gravitational and electromagnetic interactions appears to preserve reflection in space (P), time reversal (T) and charge conjugation (C) symmetries [1]. Violations of these symmetries were observed only in processes occurring by weak interactions. However, breaking of C and CP symmetries is a necessary condition for baryogenesis to occur (for generation of asymmetry between baryons and anti-baryons) [2]. Observed excess of matter over antimatter is by about nine orders of magnitude too large compared to the theoretical estimations based on known sources of discrete symmetries violation [1, 3].

Aside from the baryogenesis, excess of the matter over antimatter may be explained by the leptogenesis [4] which is the hypothesis explaining the existence of the matter in the Universe by the appearance of lepton-antilepton asymmetry in the early stage of its evolution. However, although matter is made from quarks and leptons, so far violations of CP and T symmetries have been observed only for systems including quarks - it has not yet been discovered in any processes involving purely leptonic matter [1].

Jagiellonian Positron Emission Tomography scanner (J-PET) [5–9] enables to test discrete symmetries in the decay of positronium (e^+e^-) [10, 11], which is composed of lepton-antilepton by investigating odd-symmetric operators constructed from ortho-positronium spin as well as momentum and polarization vectors of photons.

Precise determination of linear polarization of annihilation photons will also allow to investigate another enigmatic phenomenon of Nature - quantum entanglement. This property of some quantum mechanical systems is extensively studied since publication of article describing EPR paradox [12] (Albert Einstein called this feature „spooky action at the distance“ [13]). Quantum entanglement was experimentally verified in many different systems like optical photons, neutrons or K mesons but J-PET detector will be the first device to study entanglement of high energy photons and hopefully provide additional information which might be useful in developing intuitive explanation of this puzzling phenomenon of Nature [14].

Research presented in this thesis was carried out as part of the J-PET experiment with a PL-Grid infrastructure. Aim of these studies is to determine acceptance of detector as well as to check if all parameters configurations (as for example Compton scattering angles or energies) can be measured.

This thesis is organized as follows: chapter 2 contains description of detector and how it works, chapter 3 describes methods of analysis, chapter 4 is a description of conducted simulations, chapter 5 contains validation of simulations and chapter 6 contains results of those simulations.

J-PET detector

Jagiellonian Positron Emission Tomography scanner (J-PET) is being developed in order to reduce cost of device (to be affordable even by small medical facilities) by using organic scintillators instead of scintillating crystals [15–17].

2.1 Current solutions in positron emission tomography

Currently all commercial PET devices use inorganic scintillator materials as radiation detectors (usually these are the BGO (GE Healthcare), LSO (Siemens) or LYSO (Philips) crystals [18, 19]). Scintillation crystals are usually arranged in blocks with dimensions of approximately 5 cm x 5 cm and a thickness of about 2.5 cm and are additionally divided into smaller components with dimensions of about 5 mm x 5 mm. Light produced at the scintillator is converted at the rear of each block into electrical signal by photomultipliers or avalanche photo diodes (fig. 2.1). Whole PET scanner is build from approximately 144-192 blocks of such scintillator arrays (depending on the detector) [19].

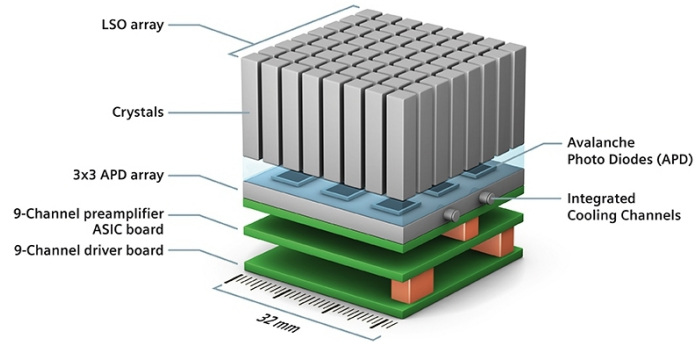


Figure 2.1: Block of scintillating crystals (4 x 4 x 20 mm) from Siemens Biograph mMR - PET/MRI scanner. The figure is adapted from Siemens web page.

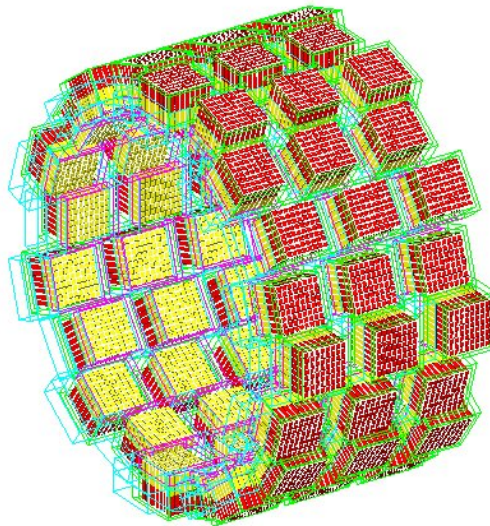
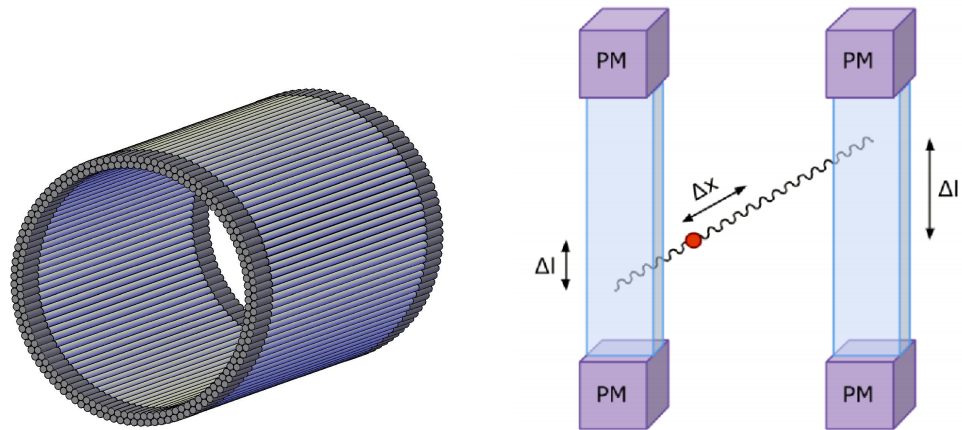


Figure 2.2: Schema of scintillator blocks arranged in a detector rings. The figure is adapted from OpenGATE Collaboration web page.

2.2 New concept

The Jagiellonian Positron Emission Tomography scanner (J-PET) is built out of axially arranged plastic scintillator strips, forming a cylinder (fig. 2.3(a)). On both ends of scintillator strip photomultipliers are connected. From time difference between signals in those photomultipliers position of interaction along strip is evaluated. Emission point is determined from time difference of annihilation quanta arrival to two strips (fig. 2.3(b)).



(a) Schematic view of the J-PET diagnostic chamber.

(b) Schematic view of the two modules of J-PET detector.

Figure 2.3: Schematics of Jagiellonian Positron Emission Tomography scanner. The figures are adapted from [5] and [1].

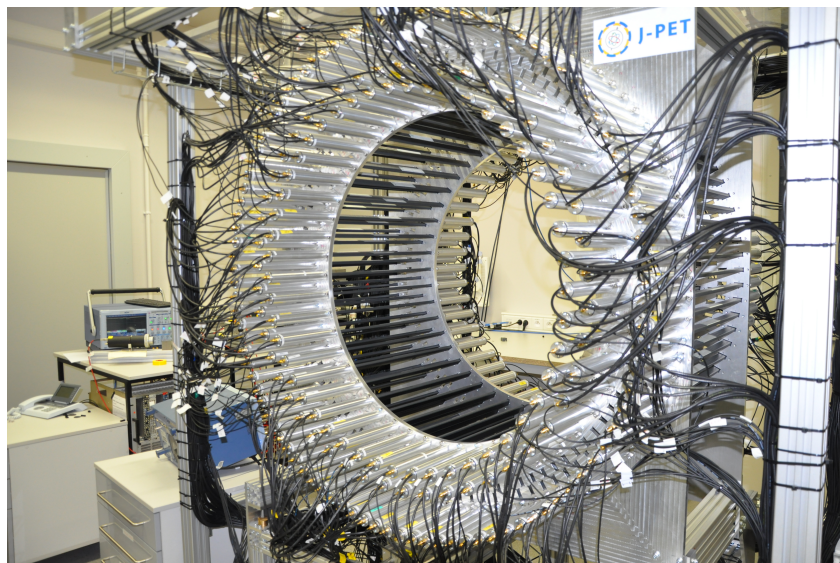


Figure 2.4: Photography of mounted prototype. The J-PET detector is made of three cylindrical layers of EJ-230 plastic scintillator strips (black) with dimension of $7 \times 19 \times 500 \text{ mm}^3$ (192 scintillators in total) and Hamamatsu R9800 vacuum tube photomultipliers (grey). The signals from photomultipliers are probed in the voltage domain at four thresholds with the accuracy of about 30 ps [20]. The figure and caption is adapted from [21].

Research methods

3.1 Positronium

Electron and positron can form a bound state exactly like electron and proton. That bound state is called positronium and is purely leptonic object. Like atoms bound by central potential it is eigenstate of parity operator P . However, unlike atoms it is also symmetric under exchange of particles into antiparticles, therefore it is an eigenstate of charge conjugation C and thus an eigenstate of CP operator. It is also the simplest atomic system with charge conjugation eigenstates [1, 22].

The ground state of positronium, like that of hydrogen atom, has two possible configurations depending on the total spin of the electron and the positron. If total spin of positronium is $S = 0$ then that state is called para-positronium (p-Ps) with a mean lifetime $\tau_{p-Ps} \approx 0.125$ ns [23]. Positronium with parallel oriented spins (with total spin $S = 1$) is known as ortho-positronium (o-Ps) and it has mean lifetime $\tau_{p-Ps} \approx 142$ ns [23].

Positronium, due to conservation of charge conjugation symmetry, can decay into even (p-Ps) or odd (o-Ps) number of gamma particles. However decays into four or more gammas are negligible - for para positronium decay into four photons have branching ratio $\approx 1.44 \cdot 10^{-6}$ and for ortho positronium decay into five photons have branching ratio $\approx 1.0 \cdot 10^{-6}$ [23].

3.2 Measurement of linear polarization of photons

J-PET scanner is build from organic scintillators, therefore photons from positronium annihilations are interacting in the detector material predominantly via Compton effect. Those scatterings are described by Klein-Nishina differential cross section [24, 25]:

$$\frac{d\sigma_{KN}}{d\Omega} = \frac{r_0^2}{2} \left(\frac{E'}{E} \right)^2 \left(\frac{E}{E'} + \frac{E'}{E} - 2 \sin^2 \theta \cos^2 \eta \right) \quad (3.1)$$

$$E' = \frac{E}{1 + \frac{E}{m_e c^2} (1 - \cos \theta)}, \quad (3.2)$$

where E is energy of incident gamma, E' energy of scattered gamma, θ denotes Compton scattering angle, r_0 stands for classical electron radius and η is angle between scattering plane (plane defined by momentum vectors of initial and scattered gamma) and electric field vector of initial gamma particle $\vec{\epsilon}$ (fig. 3.1).

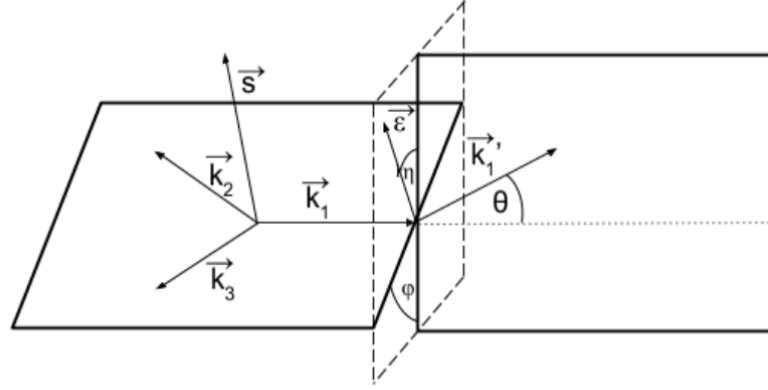


Figure 3.1: Schematic illustration of decay plane (the plane spanned on all three photons momentum vectors - \vec{k}_i) and scattering plane (formed by momentum vector of primary gamma \vec{k}_1 and scattered gamma \vec{k}_1'). Angle ϕ is an angle between those two planes, θ is Compton scattering angle and η is angle between scattering plane and linear polarization vector of photon with momentum \vec{k}_1 . Picture adapted from [1].

For low-energy photons η angle is almost always equal to 90 degree. However, when the energy increases scattering plane is not necessarily perpendicular to electric field vector, therefore precise determination of linear polarization is more complex. From Klein Nishina formula we can conclude that differential cross section (therefore probability of scattering) is maximal for $\eta = 90^\circ$ independently from initial energy and Compton scattering angle. Based on that we're assuming that electric field vector is perpendicular to scattering plane. Under this assumption we can reconstruct the direction of the polarization of the primary photon as $\vec{\epsilon} = \vec{k}_i \times \vec{k}_i'$ [1]. To estimate uncertainty of such a choice we're introducing a following procedure: Klein Nishina formula can be presented as probability density of scattering at given η angle:

$$P(E, \theta, \eta) = N(E, \theta) \cdot \frac{d\sigma_{KN}}{d\Omega}(E, \theta, \eta), \quad (3.3)$$

where $N(E, \theta)$ is normalization factor defined by integral:

$$\int_{0^\circ}^{180^\circ} N(E, \theta) \cdot \frac{d\sigma_{KN}}{d\Omega}(E, \theta, \eta) d\eta = 1 \quad (3.4)$$

The integration is in the range from 0 to 180 since we are interested only in the direction of the polarization vector and so we do not consider a sense of $\vec{\epsilon}$.

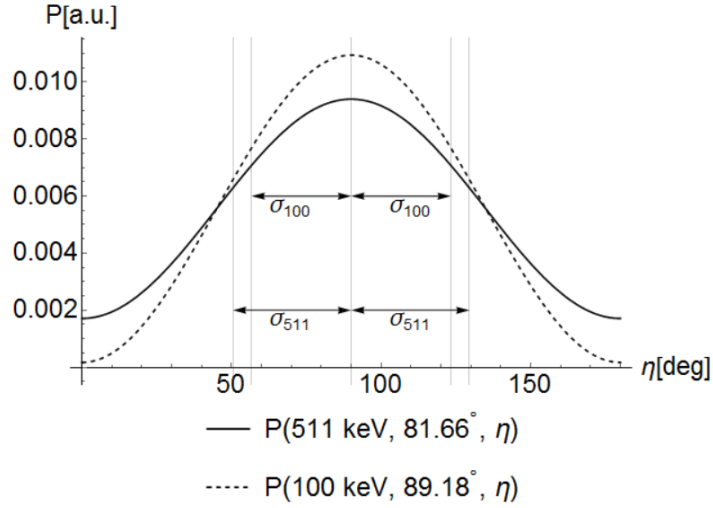


Figure 3.2: Probability density distribution as a function of η angle for two different initial energies $E = 100$ and $E = 511$ keV, at Compton scattering angles $\theta = 81, 66^\circ$ and $\theta = 89.19^\circ$ for which there is the greatest chance of scattering perpendicular to polarization of primary photon. The normalization was chosen such that the integral from 0 to 180 is equal to unity. Variable σ indicates standard deviation of the distribution (subscript correspond to initial energy). It is a measure of uncertainty of assumption that $\vec{\epsilon} = \vec{k}_i \times \vec{k}_i'$.

We can integrate that probability to receive interval of η angle in which electric vector should be found at a given probability F .

$$F(x) = \int_{90^\circ - x}^{90^\circ + x} P(E, \theta, \eta) d\eta \quad (3.5)$$

In figure 3.2 probability density of scattering at given angle η is presented for two initial energies $E = 100$ and $E = 511$ keV. Standard deviation of this distributions is denoted as σ . Parameter σ may be treated as a measure of the uncertainty of the linear polarization determination when using an assumption that $\vec{\epsilon} = \vec{k}_i \times \vec{k}_i'$. An exemplary uncertainty is illustrated pictorially in fig. 3.3 and fig. 3.4 shows σ as a function of the scattering angle and energy.

We can draw some conclusions from fig. 3.4. First, standard deviation varies from 30 to 55 degree, depending on initial energy of gamma particle as well as on the Compton scattering angle. Also, minimal standard deviation depends on energy - the higher is initial energy of gamma quanta, the higher error we make by choosing that $\vec{\epsilon} = \vec{k}_i \times \vec{k}_i'$.

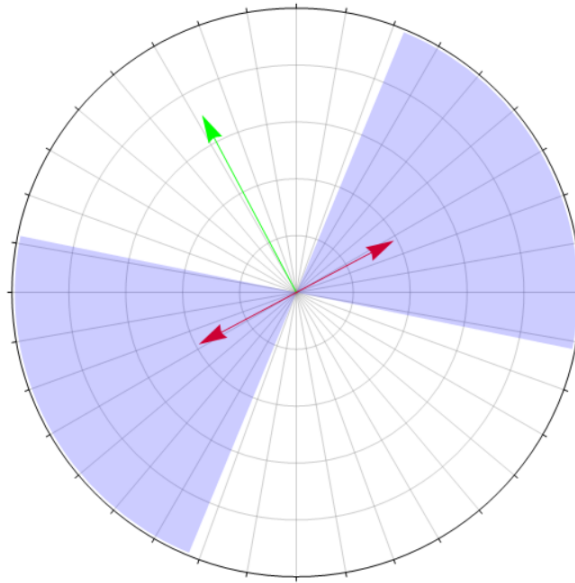
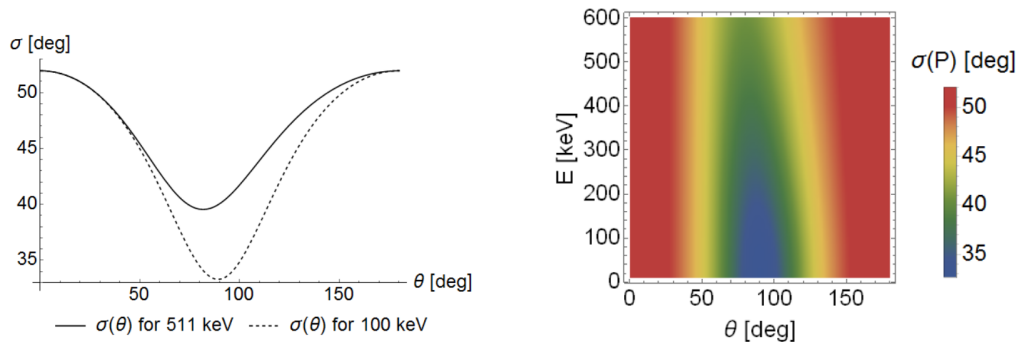


Figure 3.3: Plane perpendicular to initial photon momentum. Photon with initial momentum 511keV is scattered at Compton angle $\theta = 80^\circ$. Green arrow is a projection of scattered photon momentum, red arrows represents determined electric field vector and shaded area is area of confidence - area of one standard deviation around determined polarization. In this case that area is equal to $\pm\sigma = 39.58^\circ$.



(a) Standard deviation of fig. 3.2 as a function of Compton scattering angle for two chosen energies.

(b) Standard deviation of fig 3.2 as a function of Compton scattering angle and energy of initial gamma particle.

Figure 3.4: Standard deviation of probability density function (fig. 3.2) defined by eq. 3.3 and eq. 3.4 shown as a function of the scattering angle and energy.

Description of the simulation

Simulations were performed using GATE software [26, 27]. GATE (GEANT4 Application for Tomographic Emission) is an advanced tool developed by OpenGATE collaboration, dedicated to numerical simulations in medical imaging and radiotherapy. It uses its own macro language to configure and run simulations and provides special utilities for tomographic emission/radiotherapy like dedicated output formats or calculating dose deposited in phantom.

In order to perform simulations it was necessary to modify GATE source code and implement new functionality. First step was to incorporate possibility of simulations of ortho-positronium decays into three gamma quanta. Implementation of such source of ortho-positronium decays took place in the following manner: it was assumed that ortho-positronium is at rest and then it annihilates into photons. In simulation only four momenta of gammas are generated - not the whole process of forming, lifetime and decay of o-Ps. Special attention was paid to proper description of four-momentum distribution of emitted photons which was simulated according to the predictions derived based on the quantum electrodynamics (QED) [21, 28]. However proper spin correlations and quantum entanglement are not yet implemented.

Also, GATE software was extended to provide additional information in output file, such as four-momenta of gamma particle at each step of its path.

For the studies presented in this thesis 10^{10} events of ortho-positronium decays into three gamma quanta were simulated. Each event was simulated in the following way: i) at first three four-momenta of photons from $o\text{-Ps} \rightarrow 3\gamma$ decay was generated, ii) then interaction with matter in which photon travels is simulated for each photon, and next iii) if there is interaction of photon with the detector, information of that hit is stored in a ROOT file.

In simulation, besides the detector geometry also physical properties of plastic scintillators were taken into account. Detector consists of 192 scintillators arranged in three layers (fig. 2.4). Each scintillator is made from $EJ - 230$ (Eljen Technology) with dimensions of $500 \times 19 \times 7\text{mm}^3$

Results of this simulation, together with analysis of correlations between various quantities are presented in the following two chapters.

Validation of simulation

In order to check correctness of simulation results some tests were made. At the beginning there was prepared diagram of interaction points of gamma quanta inside the scintillator strips. Fig. 5.1 shows such distribution on a plane perpendicular to symmetry axis of J-PET scanner (fig. 5.1). This distribution was used to check if positions of registered hits correspond to positions of scintillators. Indeed as expected, the interaction points are exactly reflecting the geometrical cross section of the J-PET detector.

Position of all hits projected on XY plane

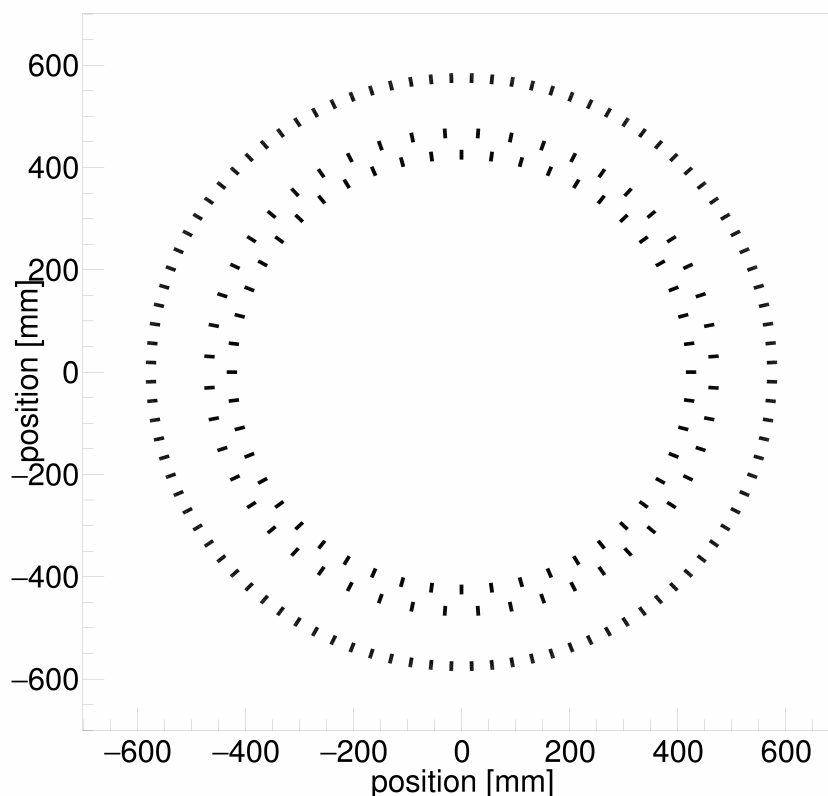


Figure 5.1: Projection of all hits onto plane perpendicular to symmetry axis of the J-PET scanner.

Next step was to check energy and angle distribution of generated gamma particles. Dalitz plot (fig. 5.4) and angles correlations (5.5) were drawn (using

notation like in fig. 5.2). For both distribution five histograms were prepared under some conditions. Histograms are build: a) for all generated events, b) for events in which all three gamma quanta are within geometrical acceptance of the detector, c) for events in which all three gamma quanta interacted in the detector, d) for events in which each gamma quantum deposited in the detector at least 30keV and e) for events in which each gamma quantum deposited in the detector at least 50keV . Histogram of energy of single gamma particle from o-Ps decay was also prepared. Those histograms were compared to theoretical distributions [21] and indeed they were in line with expectations.

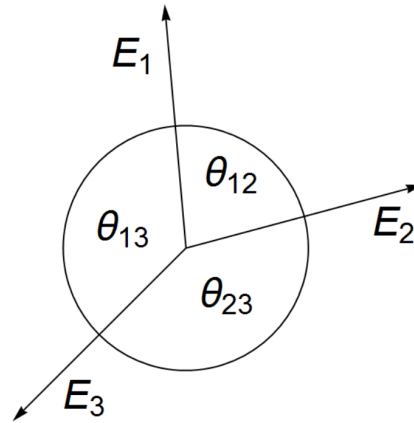


Figure 5.2: Schema of $\text{o-Ps} \rightarrow 3\gamma$ decay. E_i correspond to energy of i -th gamma quantum and θ_{ij} is an angle between momenta of i -th and j -th gamma.

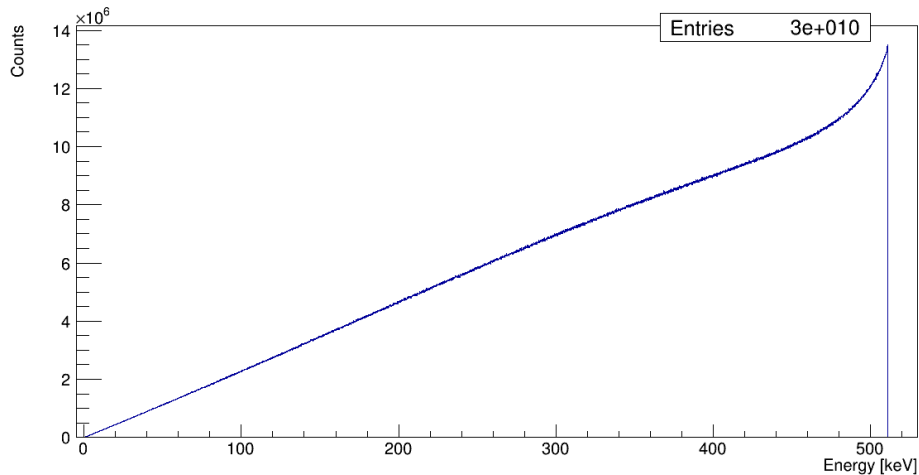
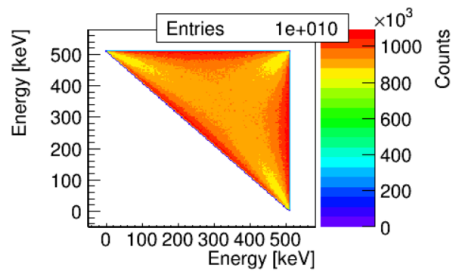
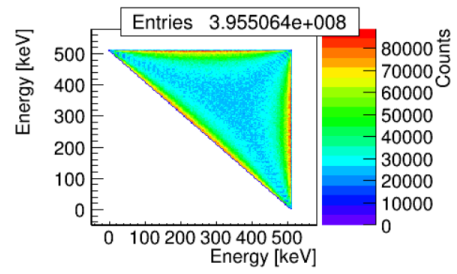


Figure 5.3: Energy distribution of single gamma particle originating from the $\text{o-Ps} \rightarrow 3\gamma$ decay.

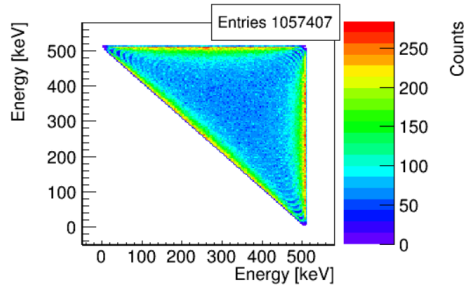
Figure 5.4(a) shows all possible energy configurations of three gamma quanta from ortho-positronium decay. From figures 5.4(b) and 5.4(c) we can conclude that detector geometry enables to detect all possible energy configurations. All of



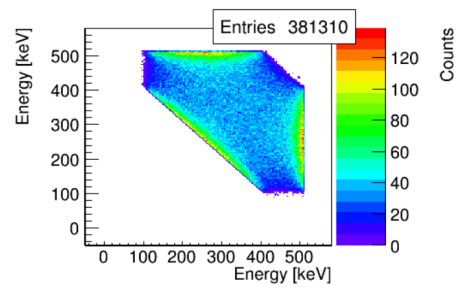
(a) E_1 vs E_2 for all generated events.



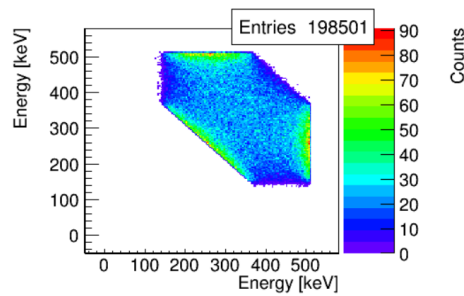
(b) E_1 vs E_2 for events in which all three gamma quanta are within geometrical acceptance of the detector.



(c) E_1 vs E_2 for events in which all three gamma quanta interacted in the detector.

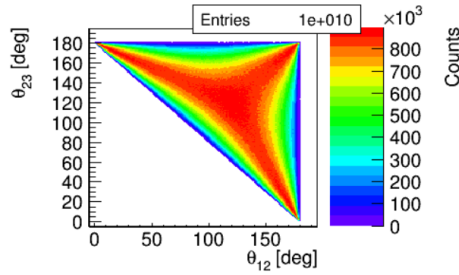


(d) E_1 vs E_2 for events in which each gamma quantum deposited in the detector at least 30keV .

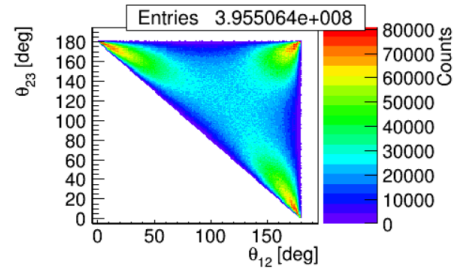


(e) E_1 vs E_2 for events in which each gamma quantum deposited in the detector at least 50keV .

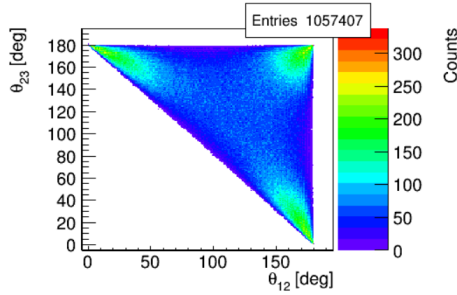
Figure 5.4: Histograms of E_1 vs E_2 for gamma quanta from the $\text{o-Ps} \rightarrow 3\gamma$ process.



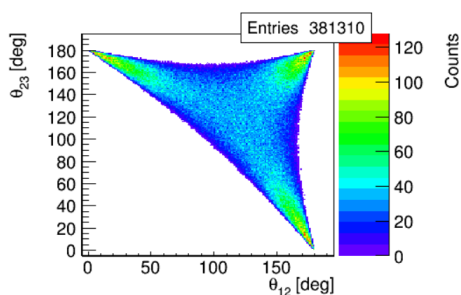
(a) θ_{12} vs θ_{23} for all generated events.



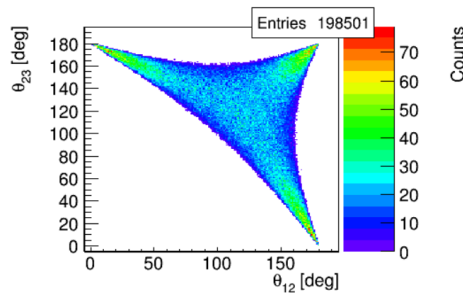
(b) θ_{12} vs θ_{23} for events in which all three gamma quanta are within geometrical acceptance of the detector.



(c) θ_{12} vs θ_{23} for events in which all three gamma quanta interacted in the detector.



(d) θ_{12} vs θ_{23} for events in which each gamma quantum deposited in the detector at least 30keV .



(e) θ_{12} vs θ_{23} for events in which each gamma quantum deposited in the detector at least 50keV .

Figure 5.5: Histograms of θ_{12} vs θ_{23} for gamma quanta from the $\text{o-Ps} \rightarrow 3\gamma$ process..

them can be measured, however the efficiency is small as can be inferred from the number of entries shown in the histograms.. Cuts on figures 5.4(d) and 5.4(e) arises from kinematic constraints. Maximal energy deposition in Compton effect occurs during back scattering (Compton scattering angle is equal to 180°). From Compton formula we can calculate minimal energy of a photon which can deposit $30keV$ - it is approximately $100keV$. If we demand that all gamma quanta must have at least that energy, we are introducing limit on available energy configurations. From momentum and energy conservation rules we can translate energy configuration to angle configuration - therefore this reasoning explains also structures observed in figures 5.5 also.

Results

Analysis of Compton scattering angles was performed (fig. 5.2). As we can see, experimentally we have access to almost all possible scattering angles (except for the smallest one). The scattering angle θ is defined at figure 3.1. It is advantageous that maximum of that distribution occurs at angles around 80 – 100 degree, that is at angles for which standard deviation (fig. 3.4) is nearly smallest.

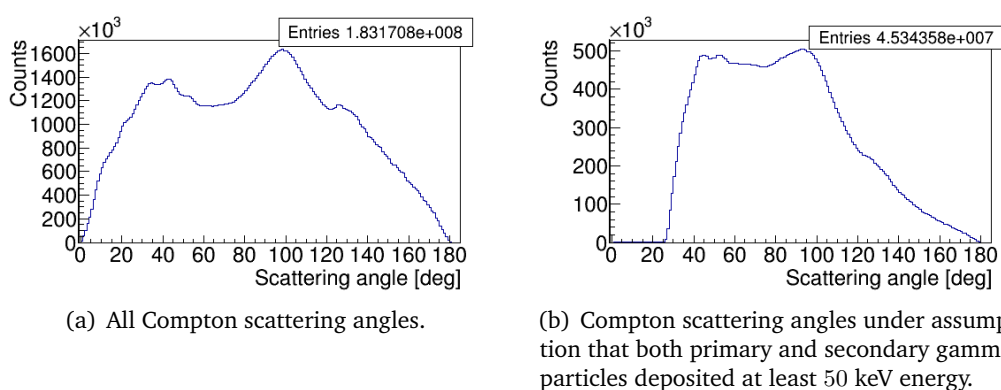


Figure 6.1: Histograms of Compton scattering angles of primary gamma quanta.

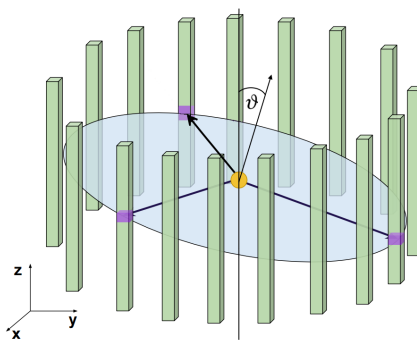
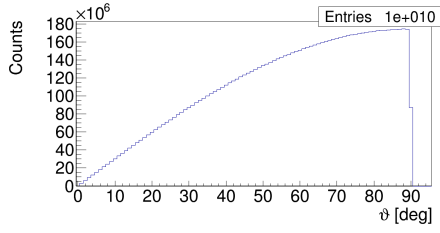
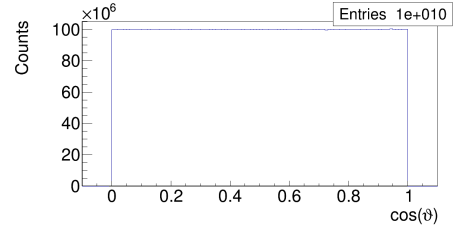


Figure 6.2: Decay plane and normal vector.

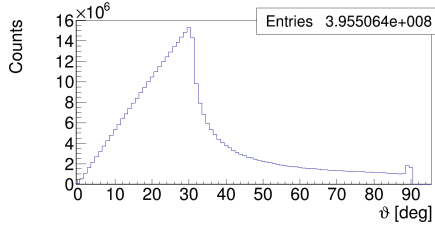
Next step was to determine which orientation of the decay planes can be measured. It was performed in the following manner: events in which all three gamma particles interact with scintillator were chosen. Then, based on points of interaction, plane on which all those three points lay was determined and normal vector to that plane was calculated (fig. 6.2). Following histograms present distribution of the angle between that vector and symmetry axis of the detector.



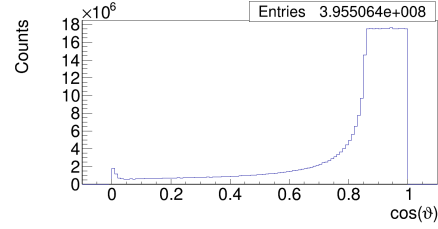
(a) Distribution of the angle ϑ between vector normal to decay plane and symmetry axis of the detector for all generated events.



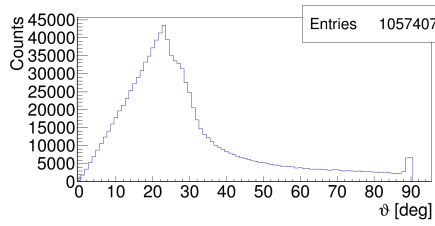
(b) Distribution of the cosine ($\cos \vartheta$) of angle between vector normal to decay plane and symmetry axis of the detector for all generated events.



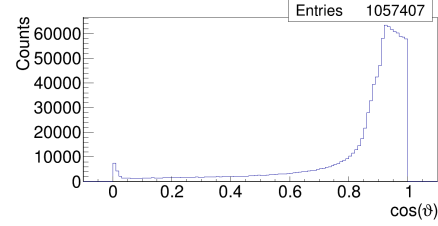
(c) Distribution of the angle ϑ between vector normal to decay plane and symmetry axis of the detector for all events in which all three gamma are in the geometrical acceptance of the detector.



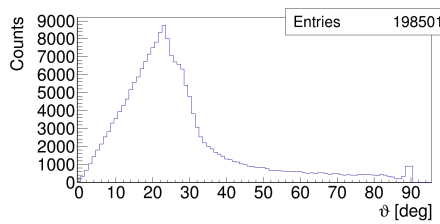
(d) Distribution of the cosine ($\cos \vartheta$) of angle between vector normal to decay plane and symmetry axis of the detector for all events in which all three gamma are in the geometrical acceptance of the detector.



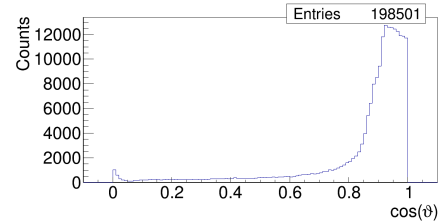
(e) Distribution of the angle ϑ between vector normal to decay plane and symmetry axis of the detector for all simulated events under assumption that all three gamma particles deposited at least 30 keV.



(f) Distribution of the cosine ($\cos \vartheta$) of angle between vector normal to decay plane and symmetry axis of the detector for all simulated events under assumption that all three gamma particles deposited at least 30 keV.



(g) Distribution of the angle ϑ between vector normal to decay plane and symmetry axis of the detector for all simulated events under assumption that all three gamma particles deposited at least 50 keV.



(h) Distribution of the cosine ($\cos \vartheta$) of angle between vector normal to decay plane and symmetry axis of the detector for all simulated events under assumption that all three gamma particles deposited at least 50 keV.

Figure 6.3: Histograms of the angle between decay plane and detector axis obtained under conditions described below the figures. Histograms are based on 10^{10} generated events.

In order to perform measurements of discrete symmetries breaking and it's further analysis it is necessary to check multiplicity of registered primary and scattered radiation. That check was performed in the following manner: for each event total number of gamma particle which scattered once (primary gamma) and twice (scattered gamma) (fig. 6.4) was calculated - represented by black line in histogram 6.5(a). The blue line shows results obtained under condition that two different primary gamma particle interacted with the same scintillator it was counted as one interaction. Similarly if two scattered gamma or if primary and scattered gamma interacted with the same scintillator it was also counted as one interaction - it is represented as a blue line. Then two different energy thresholds were applied - 30keV (each gamma particle deposited at least 30 keV energy in scintillator - red line in histogram) and 50 keV (each gamma particle deposited at least 50 keV energy in scintillator - green line in histogram). Also, histograms for only primary and only scattered gamma interactions were prepared (fig. 6.5(b) and 6.5(c) respectively).

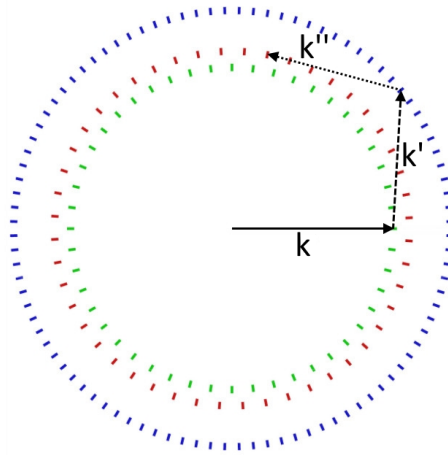
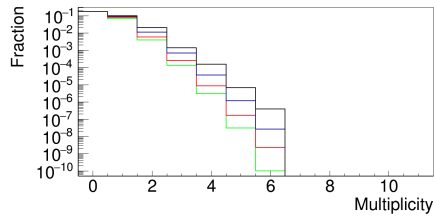


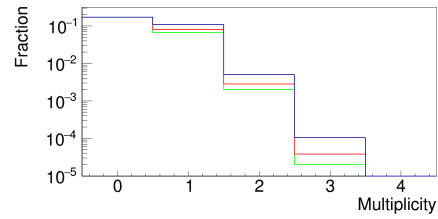
Figure 6.4: Schematic illustration of gamma particle scatterings in the detector. Primary gamma particle is gamma scattered once in a detector (vector k). Secondary gamma (vector k') is a particle scattered twice in a scintillators. We do not consider tertiary (vector k'') and further scatterings.

For studies of discrete symmetries breaking it will be necessary not only to know how many times scattered gamma quanta interacted but also if it was highest, lowest or middle energetic one. To check multiplicity of such events histogram 6.5(d) was prepared in following way: gamma particles was ordered and numbered such that $E_1 > E_2 > E_3$. Then, if all 3 gamma particles interacted with different scintillators and there was secondary scattering it was checked if it comes from first, second or third primary gamma particle and then appropriate bin in histogram was filled (energy threshold means that all three primary and one secondary gamma particle had to deposit energy at least equal to energy threshold).

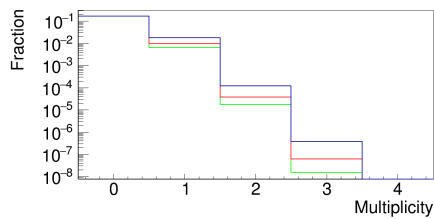
Another important information both for quantum entanglement as well as for discrete symmetries breaking studies is what angles between decay and scattering



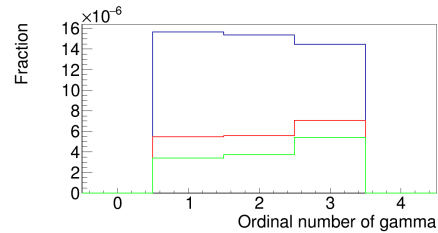
(a) Distribution of the number of all primary and secondary gamma interactions in scintillators. Black line represents event without requirement, that interactions took place in different scintillators.



(b) Distribution of the number of interactions of primary gamma particles in different scintillators.



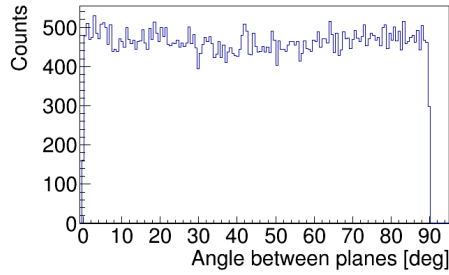
(c) Distribution of the number of interactions of scattered gamma particles in different scintillators.



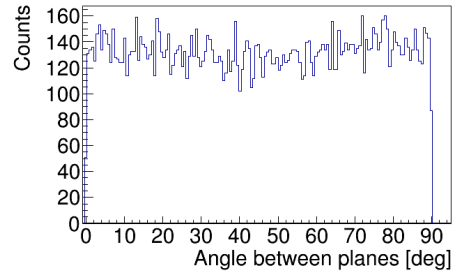
(d) Distribution of the number of interactions of i -th scattered gamma particle (primary gamma were ordered such that: $E_1 > E_2 > E_3$) under the assumption that all three primary gamma interacted in different scintillators.

Figure 6.5: Distribution of the number of interactions per event. Blue line represents all events in which interactions took place in different scintillators. Red line represents event in which energy deposited by each gamma quantum was at least 30 keV and green line that energy deposition was at least 50 keV.

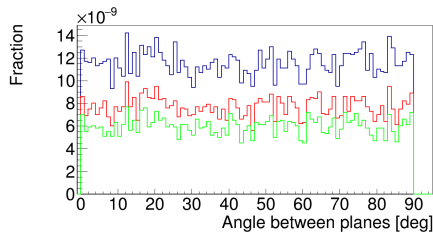
plane (fig. 3.1) we can measure and what is its distribution. Following histograms (fig. 6.6) present that distribution in a couple of cases. Gamma particles were ordered by energy in the descending order (like in histogram 6.5(d)) then, if all 3 primary gamma interacted with different scintillator, order number of registered scattered gamma was checked and angle between decay and scattering planes was calculated. Value of that angle was then written to a proper histogram.



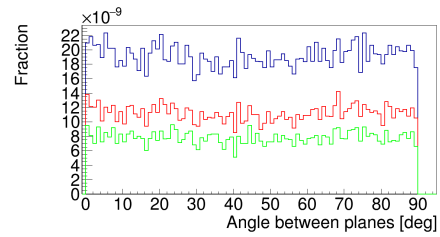
(a) Angle between decay and scattering plane for all scattered gamma particle.



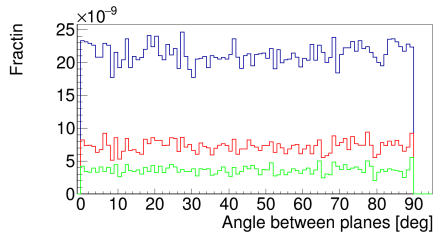
(b) Angle between decay and scattering plane for all scattered gamma particle for events in which all gamma particles deposited at least $50keV$ energy.



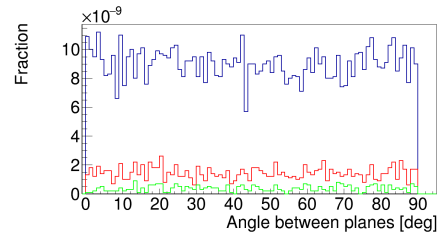
(c) Angle between decay and scattering plane for highest energetic gamma particle.



(d) Angle between decay and scattering plane for middle energetic gamma particle.



(e) Angle between decay and scattering plane for both highest and middle energetic gamma particle. Note that to make this histogram both highest and middle energetic gamma had to undergo primary and secondary scattering.



(f) Angle between decay and scattering plane for all gamma particle. Note that to make this histogram all three gamma had to undergo primary and secondary scattering.

Figure 6.6: Histograms of angle between decay and scattering planes. In order to determine that angle all three primary gamma quanta had to interact in the scintillator as well as at least one of the scattered gamma. Blue line represents number of counts without energy threshold, red line - energy threshold at level $30keV$ and green line at level $50keV$. Each bin was divided by number of events (10^{10}) to present the frequency of each angle as a fraction of all events.

6.1 Conclusions

Results of simulations are very promising for measurements of quantum entanglement and discrete symmetries breaking. Although there are some restrictions on available Compton scatterings angles it might however turn to our advantage - most of scatterings occur at Compton angle in range of $80 - 100$ degree (fig. 6.3(b)) that is

range in which we can determine linear polarization the best - therefore decreasing the uncertainty (fig 3.4).

Another important fact for quantum measurements is that in J-PET detector we are able to measure all angles between decay and scattering plane and what is more distribution of that angle is uniform and independent of energy of primary as well as scattered gamma particle (fig. 6.6).

Summary

The aim of this thesis was to analyze the feasibility of the Jagiellonian Positron Emission Tomograph (J-PET) to measure the polarisation of the gamma quanta originating from the decays of ortho-positronium atoms. In order to do so Monte Carlo simulations of such process were carried out using GATE software. Results of those simulations are very promising for measurements of quantum entanglement and discrete symmetries breaking. Although we do not have experimental access to all possible Compton scattering angles most of scatterings occur at angle in range of 80 – 100 degree (fig. 6.3(b)). That range is very convenient to measure linear polarization of annihilation gamma quanta because this is range in which we can determine linear polarization the best - therefore decreasing the uncertainty (fig 3.4). Another important fact for quantum measurements is that with the J-PET detector we are able to measure all angles between decay and scattering plane and what is more distribution of that angle is uniform and independent of energy of primary as well as scattered gamma particle (fig. 6.6).

From results of this simulation we can conclude that it is possible to measure both discrete symmetry breaking and quantum entanglement with the J-PET detector and hopefully future measurement of quantities simulated in this thesis will allow the deeper understanding of the phenomenon of quantum entanglement and to estimate the degree of discrete symmetry breaking in the leptonic sector.

Bibliography

1. Moskal, P. *et al.* Potential of the J-PET detector for studies of discrete symmetries in decays of positronium atom - a purely leptonic system. *Acta Phys. Polon.* **B47**, 509 (2016) (cit. on pp. 1, 6–8).
2. Sakharov, A. D. Violation of CP Invariance, C Asymmetry, and Baryon Asymmetry of the Universe. *Pisma Zh. Eksp. Teor. Fiz.* **5**, 32–35 (1967) (cit. on p. 1).
3. Spergel, D. N. *et al.* First year Wilkinson Microwave Anisotropy Probe (WMAP) observations: Determination of cosmological parameters. *Astrophys. J. Suppl.* **148**, 175–194 (2003) (cit. on p. 1).
4. Fukugita, M. & Yanagida, T. Baryogenesis without grand unification. *Physics Letters B* **174**, 45–47 (1986) (cit. on p. 1).
5. Moskal, P. *et al.* STRIP-PET: a novel detector concept for the TOF-PET scanner. *Nucl. Med. Rev.* **15**, C68–C69 (2012) (cit. on pp. 1, 6).
6. Moskal, P. *et al.* TOF-PET detector concept based on organic scintillators. *Nucl. Med. Rev.* **15**, C81–C84 (2012) (cit. on p. 1).
7. Moskal, P. *et al.* Test of a single module of the J-PET scanner based on plastic scintillators. *Nucl. Instrum. Meth.* **A764**, 317–321 (2014) (cit. on p. 1).
8. Moskal, P. *et al.* A novel method for the line-of-response and time-of-flight reconstruction in TOF-PET detectors based on a library of synchronized model signals. *Nucl. Instrum. Meth.* **A775**, 54–62 (2015) (cit. on p. 1).
9. Moskal, P. *et al.* Time resolution of the plastic scintillator strips with matrix photomultiplier readout for J-PET tomograph. *Phys. Med. Biol.* **61**, 2025–2047 (2016) (cit. on p. 1).
10. Kamińska, D. *et al.* Searches for discrete symmetries violation in ortho-positronium decay using the J-PET detector. *Nukleonika* **60**, 729–732 (2015) (cit. on p. 1).
11. Gajos, A. *et al.* Trilateration-based reconstruction of ortho-positronium decays into three photons with the J-PET detector. *Nucl. Instrum. Meth.* **A819**, 54–59 (2016) (cit. on p. 1).

12. Einstein, A., Podolsky, B. & Rosen, N. Can Quantum-Mechanical Description of Physical Reality Be Considered Complete? *Physical Review* **47**, 777–780 (May 1935) (cit. on p. 1).
13. Einstein, A. & Born, M. *Briefwechsel: 1916–1955. (German) [Correspondence: 1916–1955]* With contributions by Hedwig Born, with an introduction by Bertrand Russell, and with a foreword by Werner Heisenberg. Reprint of the 1969 edition. (Edition Erbrich, 1982) (cit. on p. 1).
14. Hiesmayr, B. C. Bell's theorem, the measurement problem, Newton's self-gravitation and its connections to violations of the discrete symmetries C, P, T. *J. Phys. Conf. Ser.* **631**, 012067 (2015) (cit. on p. 1).
15. Moskal, P. *Strip device and method for determining the location and time of reaction of the gamma quanta and the use of the device to determine the location and time of reaction of the gamma quanta in positron emission tomography* US Patent App. 13/383,582. 2012 (cit. on p. 3).
16. Moskal, P. *Strip device and method for determining the location and time of reaction of the gamma quanta and the use of the device to determine the location and time of reaction of the gamma quanta in positron emission tomography* EP Patent 2,454,612. 2015 (cit. on p. 3).
17. Moskal, P. *A tof-pet tomograph and a method of imaging using a tof-pet tomograph, based on a probability of production and lifetime of a positronium* WO Patent App. PCT/EP2014/068,374. 2015 (cit. on p. 3).
18. Saha, G. B. *Basics of PET Imaging: Physics, Chemistry, and Regulations* (Springer, 2014) (cit. on p. 3).
19. Slomka, P. J., Pan, T. & Germano, G. Recent Advances and Future Progress in PET Instrumentation. *Seminars in Nuclear Medicine* **46**, 5–19 (2016) (cit. on p. 3).
20. Pałka, M., Moskal, P., Bednarski, T., *et al.* A novel method based solely on field programmable gate array (FPGA) units enabling measurement of time and charge of analog signals in positron emission tomography (PET). *Bio-Algorithms and Med-Systems* **10**, 41–45 (2014) (cit. on p. 6).
21. Kamińska, D., Gajos, A., Czerwiński, E., *et al.* A feasibility study of ortho-positronium decays measurement with the J-PET scanner based on plastic scintillators. *Eur. Phys. J. C* **76**, 445 (2016) (cit. on pp. 6, 11, 14).
22. Sozzi, M. *Discrete Symmetries and CP Violation: From Experiment to Theory (Oxford Graduate Texts)* (Oxford University Press, 2012) (cit. on p. 7).
23. Karshenboim, S. G. Precision study of positronium: testing bound state QED theory. *International Journal of Modern Physics A* **19**, 3879–3896 (2004) (cit. on p. 7).

24. Evans, R. D. in *Corpuscles and Radiation in Matter II / Korpuskeln und Strahlung in Materie II* 218–298 (Springer Berlin Heidelberg, 1958) (cit. on p. 7).
25. Klein, O. & Nishina, Y. Über die Streuung von Strahlung durch freie Elektronen nach der neuen relativistischen Quantendynamik von Dirac. *Zeitschrift für Physik* **52**, 853–868 (2013) (cit. on p. 7).
26. Jan, S, Santin, G, Strul, D, *et al.* GATE: a simulation toolkit for PET and SPECT. *Physics in Medicine and Biology* **49**, 4543–4561 (2004) (cit. on p. 11).
27. Sarrut, D., Bardiès, M., Bousson, N., *et al.* A review of the use and potential of the GATE Monte Carlo simulation code for radiation therapy and dosimetry applications. *Med. Phys.* **41**, 064301 (2014) (cit. on p. 11).
28. Lifshitz, E. M. & Pitaevskii, L. P. *Relativistic Quantum Theory Part 2. Volume 4 of Course of Theoretical Physics* (Pergamon Press, 1973) (cit. on p. 11).